Spatial Imaging of Two-Dimensional Electronic States in Semiconductor Quantum Wells

K. Suzuki,[1,*] K. Kanisawa,[1] C. Janer,[1,†] S. Perraud,[1,2] K. Takashina,[1] T. Fujisawa,[1] and Y. Hirayama[1,3,4]

[1]*NTT Basic Research Laboratories, NTT Corporation, Atsugi-shi, Kanagawa 243-0198, Japan*
[2]*Laboratoire de Photonique et de Nanostructures, CNRS, 91460 Marcoussis, France*
[3]*SORST-JST, Kawaguchi-shi, Saitama 331-0012 Japan*
[4]*Tohoku University, Sendai-shi, Miyagi 980-8578, Japan*
(Received 27 December 2006; published 28 March 2007)

We measure the spatial distribution of the local density of states (LDOS) at cleaved surfaces of InAs/GaSb isolated quantum wells and double quantum wells (DQWs) by low-temperature scanning tunneling spectroscopy. Distinct standing wave patterns of LDOS corresponding to subbands are observed. These LDOS patterns and subband energies agree remarkably well with simple calculations with tip-induced band bending. Furthermore, for the DQWs, coupling of electronic states between the quantum wells is also clearly observed.

DOI: 10.1103/PhysRevLett.98.136802 PACS numbers: 73.21.Cd, 68.37.Ef, 81.05.Ea, 81.15.Hi

Scanning tunneling microscopy and spectroscopy (STM and STS) allow us to map the local density of states (LDOS), or probability amplitude (squared wave function) of electrons, in nanostructures [1,2]. By applying these techniques on semiconductors, the spatial distribution of LDOS showing the wave features of electrons has been observed around atomic steps, impurities, and in quantum dots [3–7]. However, attempts at imaging LDOS inside a semiconductor quantum well, which is one of the most fundamental quantum structures, have had limited success so far, showing only weak features that might be attributed to standing waves [8]. Imaging of LDOS in real space with nanometer resolution in heterostructures has been strongly desirable for investigating fundamental physics as well as improving device performance.

We investigate the electronic structure of InAs/GaSb heterostructures by low-temperature (LT-) STS on a cleaved surface. The InAs/GaSb system has a distinct energy band structure in which the conduction band edge of InAs can lie lower in energy than the valence band edge of GaSb. Unique physics phenomena, such as the compensated quantum Hall effect, are known to arise in this system owing to hybridization of the conduction and valence bands, making real-space analysis of the wave functions of particular interest [9,10].

In this Letter, we show spatially and energetically resolved, vivid and clear standing wave patterns of LDOS corresponding to the subbands in InAs/GaSb heterostructures. In isolated quantum wells (QWs), step-function characteristics of the density of states (DOS) for two-dimensional (2D) electronic states with expected confinement energies confirm our results. Furthermore, as a first step for applying this technique to currently used heterostructure devices with wave function coupling over layers, we image LDOS for double quantum wells (DQWs). Electronic states spread over the two layers are imaged and clear evidence of the coupling is observed. Applying this technique to other heterostructures will open further analysis, which cannot be achieved by conventional transport or optical characterization.

For QW samples, three types of multi-QWs with different InAs/GaSb layer thickness (6 nm/7 nm, 12 nm/16 nm, 17 nm/23 nm) were grown by molecular beam epitaxy on an undoped InAs (001) substrate. The GaSb barriers of these QWs are thick enough to isolate the electrons in each InAs well. All interfaces between InAs and GaSb were grown as InSb-like interfaces to obtain high quality InAs/GaSb heterostructures [11]. The schematic energy band profile is shown in Fig. 1(a).

The sample was loaded into an ultrahigh vacuum (UHV) chamber ($<2 \times 10^{-10}$ Torr) and cleaved to obtain a clean (110) surface. It is known that no surface pinning states within the energy band gap are formed on the clean (110) surface of III-V compound semiconductors. [2–4,12–14]. Then, the sample was transferred to the stage of the LT-STM without breaking the UHV condition and cooled down to $T = 4.8$ K ($k_B T \approx 0.4$ meV) to achieve high energy resolution.

Scanning was performed in UHV of the order of 10^{-11} Torr. Topographic images were obtained in constant current mode to distinguish QW structures. Figure 1(b) shows typical empty state topographic images of the 6 nm/7 nm QWs. The sample bias voltage is $V = +1$ V and the feedback current is $I = 0.1$ nA. The clear atomically resolved image indicates that the tip condition is sufficient to characterize the LDOS at nm scale. The height difference between InAs and GaSb apparent from the contrast is not a real topographic feature, but attributed to the difference in electronic structure, such as band gaps, band edge alignments, and the number of states contributing to tunneling [14]. Figure 1(c)–1(e) shows typical large area topographic images at $V = -1$ V (filled state) for each sample. No atomic steps were observable over large areas. The segregation and roughness at the interfaces, and the fluctuation of the layer thickness are small, reflecting the high quality of the heterostructures.

 © 2007 The American Physical Society

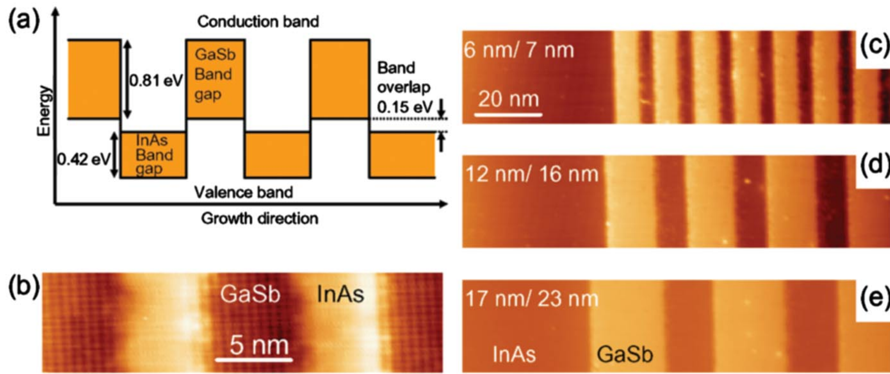

FIG. 1 (color). (a) Schematic band diagram of an InAs/GaSb heterostructure. Colored regions show the band gap. (b) Typical small area topographic image (empty state) on a cleaved cross section of InAs(6 nm)/GaSb(7 nm) quantum wells (QWs). Sample bias voltage is $V = +1$ V. Feedback current is $I = 0.1$ nA. (c)–(e) Typical large area topographic images (filled state) for 6 nm/7 nm, 12 nm/16 nm, 17 nm/23 nm QWs. $V = -1$ V, $I = 0.1$ nA. The scale is the same for all three images.

The differential tunneling conductance signal (dI/dV) was obtained using a lock-in amplifier with a small modulation of V (10 $\mathrm{mV_{pp}}$, 700 Hz). Here, STS spectra represent the normalized differential conductance $[(dI/dV)/(I/V)]$, which is known to be proportional to LDOS, as a function of V corresponding to the energy from the Fermi level [2].

Figure 2(a) and 2(b) show $(dI/dV)/(I/V)$ curves as a function of V at the center of the InAs and GaSb layers, respectively, for the 17 nm/23 nm QWs. Blue regions correspond to the band gap. For the InAs layer, the conduction band bottom lies below the Fermi level at $V = 0$ V, because electrons are accumulated in the InAs layer due to charge transfer from the GaSb. In contrast to the InAs spectrum, the valence band top for the GaSb almost coincides with the Fermi level position, because the valence band, which has a flatter dispersion relation, can accommodate holes accumulated in the GaSb layer within a small energy interval [10].

The spatial variation of the STS spectra for the 17 nm/23 nm QWs is shown as a function of the relative position along the growth direction in Fig. 2(c). The red (blue) regions show higher (lower) normalized differential conductance corresponding to high (low) LDOS. The distinct energy band profile shown in Fig. 1(a) is well reproduced in Fig. 2(c).

Now, we focus on electronic structure in the InAs conduction band region [circle in Fig. 2(c)]. Figure 3(a) shows STS spectra with higher spatial and energy resolution for each V from 0.01 V to 0.9 V with a step of 0.01 V, which is also shown in the color scale plot of Fig. 3(c). The number of oscillations in LDOS increases with V (energy), indicating that there are standing wave patterns due to the confined subbands in the QW. Figure 3(d) shows the DOS obtained by integrating the LDOS over the QW region. Steplike features are observed when the number of LDOS oscillations increase, as shown by lines in Fig. 3(c) and 3(d). This is characteristic of a 2D extended system where each subband contributes a constant DOS leading to steps, in turn verifying that they are not states localized at the cleaved surface.

Similarly, for the 12 nm/16 nm QWs, clear standing wave patterns were also observed in Fig. 3(e). The energy levels for each subband are higher and the energy differences between subbands are larger than those for the 17 nm/23 nm QWs, demonstrating the stronger confinement [Fig. 4(b)]. For the 6 nm/7 nm QWs, the boundary between the ground and second subbands is observed clearly in this energy region [Fig. 3(f)]. The second subband in each InAs layer starts at different energy due to monolayer-scale layer thickness fluctuations ($\sim\pm 0.02$ eV).

We now compare the STS spectra with a simple calculation for a single quantum well. A sheet carrier density of $1 \times 10^{16}\ \mathrm{m^{-2}}$, which is a typical value for InAs/GaSb heterostructures, is taken for 17 nm/23 nm and 12 nm/16 nm QWs, and zero for 6 nm/7 nm QWs [15]. The band nonparabolicity is taken to be $m^*(E) = m^*_{\mathrm{bulk}}(1 + 2E/E_g)$, where $m^*_{\mathrm{bulk}} = 0.023m_0$ is the effective mass at the conduction band bottom of bulk InAs, E is the energy measured from the InAs conduction band bottom, and $E_g = 0.42$ eV is the InAs band gap energy. The InAs conduction band bottom is set to be 0.15 eV below the Fermi level [9]. Using a total potential barrier height of 0.96 eV (GaSb band gap is 0.81 eV), we calculated the subband energies, wave function distribution, and potential profile solving the Schrödinger and Poisson equations self-consistently. Since each subband possesses 2D translational kinetic degrees of freedom, subbands from the first (ground) to the nth contribute to the tunneling at the

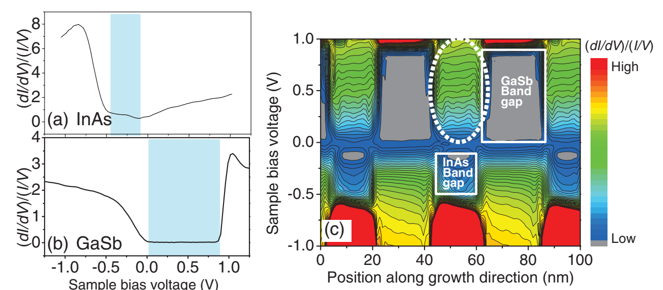

FIG. 2 (color). Normalized differential tunneling conductance $[(dI/dV)/(I/V)]$ as a function of the sample bias voltage (V) at the center of an InAs layer (a) and a GaSb layer (b) for 17 nm/23 nm QWs. The data were averaged along lines parallel to the interface. Blue regions show the band gap. (c) Color contour plot of the spatial variation of the STS spectra.

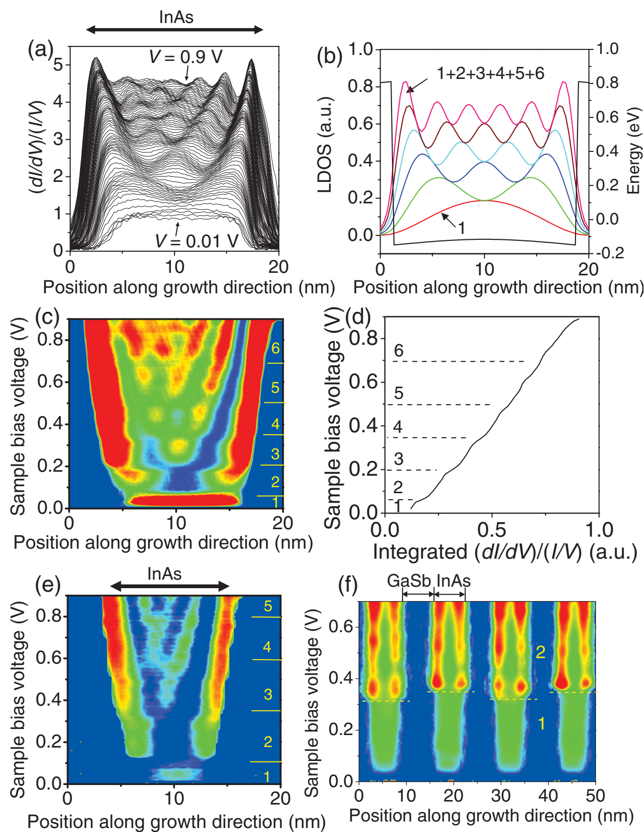

FIG. 3 (color). (a) High spatial and energy resolution STS spectra for 17 nm/23 nm QW, focusing on the white dotted circle in Fig. 2(c). $(dI/dV)/(I/V)$ curves are plotted for each V with a step of 0.01 V. (b) Calculated LDOS spectra taken to be the sum of the squared wave functions for subbands. The conduction band potential profile modulated by the electron accumulation in the well is overlaid. (c) Enhanced STS spectra. In the InAs layer, oscillation minima in $(dI/dV)/(I/V)$ curves as a function of the position along the growth direction at each V are set to zero. The subband indices are indicated. (d) Experimentally deduced electron density of states: each $(dI/dV)/(I/V)$ curve in (a) is integrated over the quantum well. (e) Enhanced STS spectra for 12 nm/15 nm QW. (f) STS spectra for 6 nm/7 nm QW.

voltage corresponding to the nth subband. Therefore, the nth LDOS spectrum can be considered as a sum of the squared wave functions for the contributing subbands. Figure 3(b) shows the calculated LDOS spectra for a 17 nm/23 nm QW as a function of the position along the growth direction with the conduction band potential profile. The calculated LDOS spectra reproduces the shape of the observed STS spectra in Fig. 3(a) well.

Calculated subband energies for each QW are shown in Fig. 4(a)–4(c). Observed subband energies are also plotted. For all subbands, observed energies are larger than the calculated energies and the difference becomes greater with increasing subband indices. In Fig. 4(d), the difference is plotted as a function of the energy. The difference is increasing linearly.

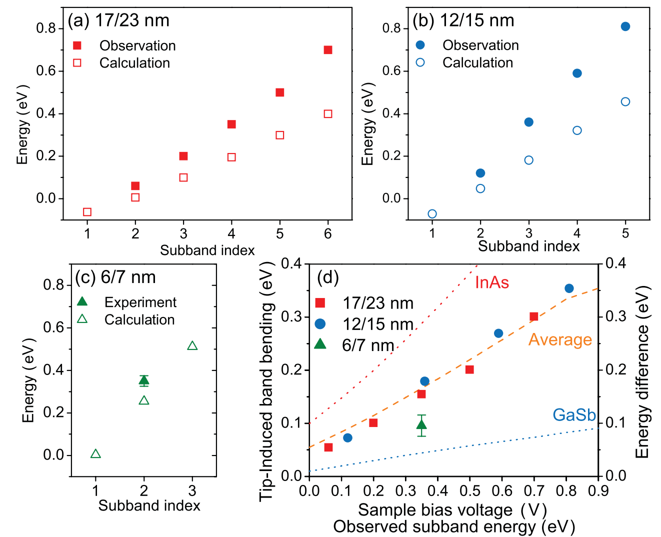

FIG. 4 (color). (a)–(c) Comparison between observed and calculated subband energies. (d) The differences between observed and calculated subband energies as a function of the observed subband energy. Tip-induced band bending as a function of V calculated for InAs and GaSb independently (dotted lines) and averaged (dashed line).

To explain the energy difference between the above calculation and the observation, consideration of tip-induced band bending is essential [2–4,12,13]. For samples with an unpinned Fermi level on the cleaved (110) surface, the spatial charge distribution near the surface is modified by the electric field from the STM tip. We calculated this effect of the tip-induced band bending using a simple one-dimensional model [13,16] with reasonable values for fitting parameters (work function of the tungten tip: 5.0 eV [17], the tip-sample distance: 1.00 nm [13], donor density for InAs: 1×10^{24} m^{-3}, and acceptor density for GaSb: 1×10^{24} m^{-3} [18]). Since the effective diameter of the STM tip is approximately 100 nm, which is much greater than our QW thicknesses, the band bending should be present continuously over the entire observed region [19]. Therefore, we calculated the effect for the InAs and GaSb layers independently and took an average as plotted in Fig. 4(d). The calculation coincides with the observed energy difference [20], showing that the observable LDOS originate from the 2D electronic states influenced by the tip-induced band bending.

In order to test the imaging for coupling between the electronic structures of two neighboring InAs QWs, we have investigated LDOS in DQW samples with slight asymmetry in the well widths. The slight asymmetry simplifies the identification of observed subbands and the role of coupling since the subband degeneracy is lifted and it becomes clear which QW mainly contributes to the resulting coupled subbands. The STM topographic image for a DQW shown in Fig. 5(a) indicates asymmetric wells with 4.8 and 5.4 nm thicknesses and a 0.9 nm thick GaSb central barrier layer. The STS spectra are shown in Fig. 5(b). In

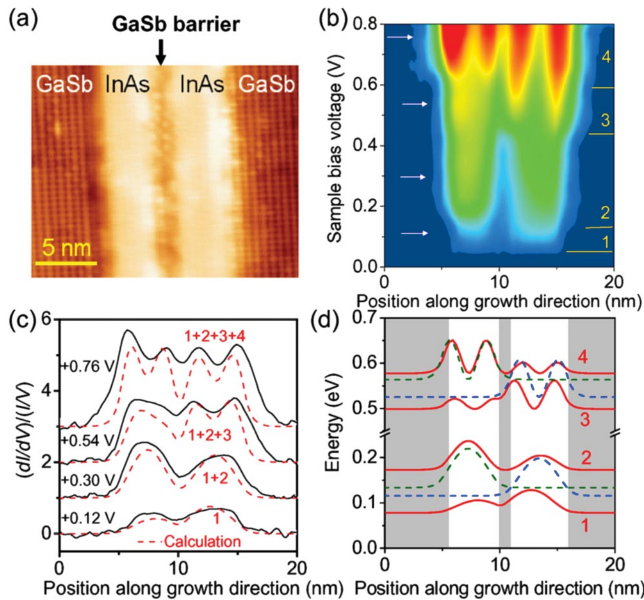

FIG. 5 (color). (a) STM topographic image of a DQW ($V = +1$ V). (b) STS spectra. (c) $(dI/dV)/(I/V)$ curves at voltages arrowed in (b) (offset). Red dashed lines are calculated LDOS. (d) Calculated squared wave functions (solid lines) and subband energies (offset) for the DQW (red). Those for 4.8 nm (green dashed line) and 5.4 nm (blue dashed line) single QWs are also shown for comparison.

contrast to the isolated QWs, standing wave patterns extend over both InAs layers. The pattern changes abruptly at 0.06, 0.14, 0.46, and 0.60 V shown by solid lines, which indicate the onset of the subbands. Representative $(dI/dV)/(I/V)$ curves for each subband at the arrowed voltages are shown in Fig. 5(c). The number of peaks in the LDOS pattern is two for the ground and second subbands, three for the third subband, and four for the fourth subband. The DOS is weighted to the right (thicker) well for the ground subband, and to the left (thinner) well for the second subband.

Figure 5(d) shows calculated squared wave functions (red solid lines) and energies (offset) for each subband using a rectangular DQW potential. The averaged tip-induced band bending [Fig. 4(d)] is included in the energy scale. The observed $(dI/dV)/(I/V)$ curves in Fig. 5(c) agree well with the calculated LDOS spectra (dashed lines) for the coupled DQW rather than independent single QWs, verifying that the observed LDOS directly reflects the wave functions of a coupled system, distributed over both QWs.

In conclusion, we have investigated the local electronic structure in InAs/GaSb isolated QWs and DQWs by LT-STS on a cleaved cross sectional surface. Expected energy band profiles were clearly seen in the STS spectra. Clear images of standing waves of LDOS corresponding to the subbands were obtained as a function of the energy. The standing wave patterns agree remarkably well with the calculated LDOS. For QWs, the observed subband energies were well explained by a single quantum well model with tip-induced band bending. For a DQW slight difference in the InAs well thicknesses is reflected in the asymmetric STS spectra. The coupling effect between the InAs wells was clearly observed.

We are grateful to H. Yamaguchi and M. Ueki for fruitful discussion and sample growth. This work was partly supported by a Grant in Aid for Scientific Research from the Japan Society for the Promotion of Science, JSPS KAKENHI (No. 16206003).

*Electronic address: kyoichi@will.brl.ntt.co.jp
†On leave from Ecole Supérieure de Physique et de Chimie Industrielles, 75005 Paris, France.

[1] G. Binning, H. Rohrer, Ch. Gerber, and E. Weibel, Phys. Rev. Lett. **49**, 57 (1982).
[2] R. M. Feenstra, Phys. Rev. B **50**, 4561 (1994).
[3] M. C. M. M. van der Wielen, A. J. A. van Roij, and H. van Kempen, Phys. Rev. Lett. **76**, 1075 (1996).
[4] R. Dombrowski, Chr. Wittneven, M. Morgenstern, and R. Wiesendanger, Appl. Phys. A **66**, S203 (1998).
[5] K. Kanisawa, M. J. Butcher, H. Yamaguchi, and Y. Hirayama, Phys. Rev. Lett. **86**, 3384 (2001).
[6] K. Kanisawa, M. J. Butcher, Y. Tokura, H. Yamaguchi, and Y. Hirayama, Phys. Rev. Lett. **87**, 196804 (2001).
[7] T. Maltezopoulos, A. Bolz, C. Meyer, C. Heyn, W. Hansen, M. Morgenstern, and R. Wiesendanger, Phys. Rev. Lett. **91**, 196804 (2003).
[8] R. M. Feenstra, D. A. Collins, D. Z.-Y. Ting, M. W. Wang, and T. C. McGill, J. Vac. Sci. Technol. B **12**, 2592 (1994).
[9] E. E. Mendez, L. Esaki, and L. L. Chang, Phys. Rev. Lett. **55**, 2216 (1985).
[10] K. Suzuki, K. Takashina, S. Miyashita, and Y. Hirayama, Phys. Rev. Lett. **93**, 016803 (2004).
[11] G. Tuttle, H. Kroemer, and J. H. English, J. Appl. Phys. **67**, 3032 (1990).
[12] G. M. Guichar, C. A. Sebenne, and G. A. Garry, Phys. Rev. Lett. **37**, 1158 (1976).
[13] R. M. Feenstra and J. A. Stroscio, J. Vac. Sci. Technol. B **5**, 923 (1987).
[14] S. G. Kim, S. C. Erwin, B. Z. Nosho, and L. J. Whitman, Phys. Rev. B **67**, 121306(R) (2003).
[15] H. Munekata, E. E. Mendez, Y. Iye, and L. Esaki, Surf. Sci. **174**, 449 (1986).
[16] R. Seiwatz and M. Green, J. Appl. Phys. **29**, 1034 (1958).
[17] *CRC Handbook of Chemistry and Physics*, edited by D. R. Lide (CRC Press, Boca Raton, 1998), 79th ed., pp. 12–24.
[18] E. E. Mendez, L. L. Chang, C.-A. Chang, L. F. Alexander, and L. Esaki, Surf. Sci. **142**, 215 (1984).
[19] The expected tip radius is in the range $d = 20$–40 nm, Y. Dong, R. M. Feenstra, R. Hey, and K. H. Ploog, J. Vac. Sci. Technol. B **20**, 1677 (2002). We used $2\sqrt{3}d$ as the effective tip diameter, which is the carry of an electric field line launched from the spherical tip parallel to the plane.
[20] The small discrepancy for 6 nm/7 nm QWs may be attributed to the effect of the large effective mass in the GaSb barriers, which is not considered in the calculation, because of the large penetration of the wave functions into the barriers.